Contents lists available at ScienceDirect

Applied Catalysis B: Environmental

journal homepage: www.elsevier.com/locate/apcatb

Synergistic effect of photocatalysis and thermocatalysis for selective oxidation of aromatic alcohols to aromatic aldehydes using $Zn_3In_2S_6$@ZnO composite

Jinghu Zhang [a,b], Sugang Meng [a,**], Xiangju Ye [b,**], Cancan Ling [a,b], Sujuan Zhang [a], Xianliang Fu [a], Shifu Chen [a,b,*]

[a] Department of Chemistry, Huaibei Normal University, Anhui Huaibei, 235000, People's Republic of China
[b] Department of Chemistry, University of Science and Technology of Anhui, Anhui Fengyang, 233100, People's Republic of China

ARTICLE INFO

ABSTRACT

Selective oxidation of aromatic alcohols to corresponding carbonyl compounds under mild conditions has a promising prospect in industry. In the paper, we successfully prepared a new mode of photothermocatalyst, $Zn_3In_2S_6$@ZnO composite, which shows dramatically enhanced activity for selective oxidation of benzyl alcohol to benzaldehyde compared with single $Zn_3In_2S_6$ and ZnO under visible light illumination. The enhancement is due to a synergistic effect of low-temperature thermocatalysis on ZnO and photocatalysis on $Zn_3In_2S_6$. ZnO could weaken bonds of the C—H_α and the O—H. Then the reactive species ($^\bullet O_2{}^-$ and h$^+$) generated on $Zn_3In_2S_6$ could be easy for selective oxidation of benzyl alcohol to produce benzaldehyde. The photoelectrochemical and photoluminescence (PL) results and a series of control experiments (e.g. reaction temperature and radical scavenger) prove this synergistic effect and proposed mechanism. Moreover, the stable performance and high activity of $Zn_3In_2S_6$@ZnO for other aromatic alcohols indicate its applicable potential. This study provides a promising way to combine photocatalysis and thermocatalysis for the design of novel and efficient visible-light-driven catalyst for selective oxidation of aromatic alcohols or other organics under mild reaction conditions.

© 2017 Elsevier B.V. All rights reserved.

1. Introduction

Since Fujishima and Honda found that water can be split into H_2 and O_2 by a TiO_2 electrode under UV-light irradiation in 1972 year [1], numerous types of materials have been developed as photocatalysts, such as metallic oxides [2], metal sulfides [3], metal-free semiconductors [4], composites [5], etc. [6,7]. Many reports published had proved that the photocatalysis method has a great promise for environmental remediation [2], solar energy conversion [3,7], and organics transformation [8,9] and so on [7,10]. In recent years, the photocatalytic selective oxidation of aromatic alcohols to corresponding aldehydes has attracted extensive attention [10], because such aromatic aldehydes and their derivatives are crucial raw materials for the synthesis of fine chemicals and pharmaceuticals [11]. The traditional preparation methods of aromatic

aldehydes (chemical oxidation treatment and thermocatalysis) have serious drawbacks (using toxic or corrosive stoichiometric oxidants such as $KMnO_4$, Cr^{IV}, ClO^- and Cl_2, expending vast energy to provide the unavoidable temperature and pressure, causing environment pollution, etc.) [12]. It is known that the photocatalysis method can remedy these defects efficiently, because of its high selectivity, use of solar light as the driving force and O_2 as an oxidant, the milder reaction conditions and environmentally friendly properties [12]. However, in order to achieve the industrialization, the prepared photocatalysts excited by visible-light and with high activity is the key factor for the photocatalytic selective organic transformation.

It has been reported that TiO_2 is one of the most promising photocatalysts because of its low costs, easy availability, high photocatalytic activity, and so on [1–3]. However, it has been confirmed that benzyl alcohol could be oxidized immoderately to yield benzoic acid or carbon dioxide because of its powerful oxidizing capacity [12,13]. Meanwhile, the wide band gap (3.2 eV) is another factor to limit the application [5], because the UV-light that only occupied 7% in sunlight can be absorbed by TiO_2. Therefore, great efforts have been devoted in order to enhance the utilization of

visible light and improve the selectivity to target product. For example, modifying TiO_2 through doping ions [14] and coupling with noble metals [15] or other semiconductors [16], and developing non-TiO_2 photocatalysts such as $ZnIn_2S_4$ [17], In_2S_3 [18], g-C_3N_4 [19], $Bi_{12}O_{17}Cl_2$ [13], MVO_4 (M = In, Bi) [8] etc. [9,10]. In despite of these advances in the photocatalytic selective transformation of aromatic alcohols, the design of an efficient and stable photocatalyst for selective oxidation of aromatic alcohols into aromatic aldehydes under visible light has remained challenges so far.

It is well known that transformation of aromatic alcohols into corresponding aldehydes is a dehydrogenation process. It has been reported that ZnO was frequently studied as a promising thermocatalyst for dehydrogenation of alcohols [20–22]. For example, Antonio Guerrero-Ruiz et al. [21] reported that ZnO showed high activity (selectivity of 94%) for the thermocatalytic dehydrogenation of ethanol into acetaldehyde at 623 K for 1 h. Y. Shinohara et al. [22] studied the dehydrogenation of 2-propanol by experiments and theory. The results showed that the selectivity of ZnO for the dehydrogenation of 2-propanol could reach up to 97.8% at 523 K. On the other hand, Zn-In-S (e.g. $ZnIn_2S_4$ and $Zn_3In_2S_6$), an important ternary semiconductor, is of great interest to applications such as energy conversion and the photocatalysis due to its direct band gap (2.4–2.8 eV for bulk materials) and outstanding optical and electrical properties [23]. For example, $ZnIn_2S_4$ and $Zn_3In_2S_6$ showed high activities for H_2 evolution under visible light irradiation [24]. Moreover, $ZnIn_2S_4$ could be employed as catalyst to activate O_2 for selective oxidation of aromatic alcohols into aromatic aldehydes under visible light [17a]. Therefore, $Zn_3In_2S_6$ may be an excellent photocatalyst for selective oxidation of aromatic alcohols. However, few of the literature about the properties of $Zn_3In_2S_6$ as a photocatalyst have been reported for photocatalytic selective organic transformation. According to the above analysis, if a dehydrogenation catalyst (e.g. ZnO) is combined with a photocatalyst (e.g. $Zn_3In_2S_6$), a visible-light excited, efficient and stable catalyst for selective oxidation of aromatic alcohols to corresponding aldehydes may be produced. This is first time to report the synergistic effect of the photocatalysis and thermocatalysis for selective oxidation of aromatic alcohols into aromatic aldehydes.

In this paper, a novel mode of catalysts of $Zn_3In_2S_6$@ZnO composite for selective oxidation of aromatic alcohols to corresponding aldehydes, which possess both photocatalytic and thermocatalytic activities, was prepared by a hydrothermal method and a solvent assisted interfacial reaction. The composite $Zn_3In_2S_6$@ZnO exhibits an efficient synergistic effect for selective oxidation of aromatic alcohols to corresponding aromatic aldehydes under mild conditions by photothermocatalytic reaction. In the $Zn_3In_2S_6$@ZnO composite, $Zn_3In_2S_6$ as a photocatalyst was motivated under visible light illumination to generate the reactive species (electrons, holes and superoxide radical), and ZnO as a thermocatalyst loaded on the surface of $Zn_3In_2S_6$ could weaken the bonds of C—H_α and O—H of benzyl alcohol (PhCH$_{\alpha2}$OH) by low-temperature thermocatalysis [22]. The physical, chemical and photoelectric properties of $Zn_3In_2S_6$@ZnO composite were characterized by XRD, UV–vis DRS, SEM, TEM, EDS-mapping, XPS and BET techniques. The photothermocatalytic synergistic effect was thoroughly investigated by photoelectrochemical, PL and a series of control experiments. A possible reaction mechanism was proposed.

2. Experimental

2.1. Materials

Indium chloride tetrahydrate ($InCl_3\cdot4H_2O$), thiacetamide (CH_3CSNH_2), zinc sulfate heptahydrate ($ZnSO_4\cdot7H_2O$), zinc acetate ($ZnAc_2$), potassium hydroxide (KOH) and methanol (CH_3OH) were purchased from by Aladdin Chemistry Co. (Shanghai, China). All chemicals used in the experiments were analytical pure grade and used directly without further purification.

2.2. Preparation of samples

2.2.1. Synthesis of $Zn_3In_2S_6$ sample

$Zn_3In_2S_6$ was prepared by a modified hydrothermal method [24]. In a typical procedure, 2 mmol $InCl_3\cdot4H_2O$, 3 mmol $ZnSO_4\cdot7H_2O$ and a double excess of CH_3CSNH_2 were dissolved in 70 mL of deionized water. The mixed solution was further transferred into a 100 mL Teflon-lined autoclave. The autoclave was sealed and heated at 433.15 K for 12 h, and then cooled down to room temperature. A light yellow precipitate was washed with absolute ethanol and deionized water for several times. Finally, the obtained product was dried in a vacuum oven at 333.15 K for 8 h.

2.2.2. Synthesis of $Zn_3In_2S_6$@ZnO composites and ZnO sample

The as-prepared $Zn_3In_2S_6$ powder was added into 15 mL methanol, then 0.1 M $ZnAc_2$ methanol solution was added dropwise into the $Zn_3In_2S_6$ suspension to form mixed suspension under continuous stirring at 333.15 K. After vigorous stirring for 30 min, double stoichiometric ratio of KOH was added into the above suspension and maintained at 333.15 K for 2 h. Then the mixed suspension was allowed cooling to room temperature. The yellowish product was collected by a centrifugal machine, washed thoroughly with deionized water, and dried in a vacuum oven at 333.15 K for 8 h. For comparison, ZnO was prepared by the similar procedure without adding $Zn_3In_2S_6$.

2.3. Characterization

X-ray diffraction (XRD) was recorded by a Bruker D8 advance X-Ray powder diffractometer with Cu Kα radiation and a scanning speed of $3° min^{-1}$ at room temperature. UV–vis diffuse reflectance spectroscopy (DRS) was carried out to measure the optical properties of the as-prepared samples by a UV–VIS-NIR spectrophotometer (UV-3600, SHIMA-DZU, Japan) with $BaSO_4$ as a reflectance standard. The morphologies and microstructures of the photocatalysts were investigated by scanning electron microcopy (SEM, Hitachi S4800) and transmission electron microscopy (TEM, FEI Tecnai G2 F20). N_2 adsorption-desorption isotherms and the Brunauer-Emmett-Teller (BET) surface areas were measured with an ASAP 3020 system (Micromeritics Instrument Corp.). The X-ray photoelectron spectroscopy (XPS) measurement was performed on a Thermo Scientific ESCA Lab250 spectrometer with an Al Kα X-ray beam, and the binding energies were corrected with reference to C 1s peak at 284.6 eV. Photoluminescence (PL) experiments were carried out by the FP-6500 fluorescence spectrometer. The value of ZnO amount in $Zn_3In_2S_6$@ZnO composites was measured by inductively coupled plasma-mass spectrometry (ICP-MS, X-Series 2, Thermo Fisher Scientific, Germany.).

The photoelectrochemical experiments were performed in a three-electrode system (CHI-660E, Chenhua Instruments Co. Shanghai, China). A Pt wire and Ag/AgCl were used as counter electrode and reference electrode, respectively. The catalyst powder was deposited on the fluoride tin oxide (FTO) substrate to serve as working electrode. A quartz cell filled with 0.1 M Na_2SO_4 or 0.1 M KCl electrolyte containing 0.1 M $K_3[Fe(CN)_6]$/$K_4[Fe(CN)_6]$ was used as the reaction system. A 300 W Xenon lamp (PLS-SXE 300C, Beijing Perfect Light Co. Ltd) equipped with a 420 nm cutoff filter (λ > 420 nm) was applied as a visible light source.

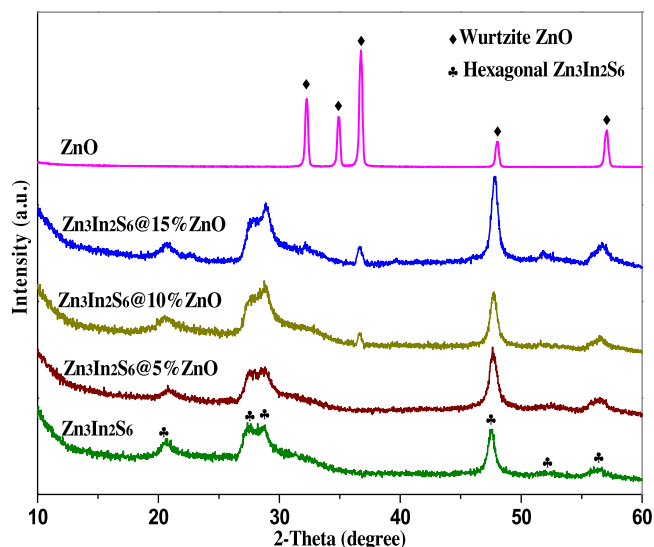**Fig. 1.** XRD patterns of pure ZnO, $Zn_3In_2S_6$ and $Zn_3In_2S_6$@ZnO composites.

2.4. Evaluation of catalytic activity

The catalytic activity of the samples for selective oxidation of aromatic alcohols to corresponding aromatic aldehydes was performed in a 100 mL of Teflon-lined stainless steel autoclave with a pressure gage. It has been reported in our previous studies [18]. The reaction equipment may be placed in a heating jacket or in a circulating condensate unit as desired. For each measurement, 80 mg catalyst and 0.5 mmol aromatic alcohols were dispersed in 15 mL benzotrifluoride (BTF). Before illumination, the autoclave was filled with O_2 at a pressure of 0.1 MPa, and the mixed suspension was stirred for 30 min to attain the equilibrium of adsorption-desorption. A 300W Xenon lamp (PLS-SXE 300C, Beijing Perfect Light Co. Ltd) equipped with a 420 nm cutoff filter ($\lambda > 420$ nm) was applied as a visible light source. After the reaction, the mixture was centrifuged to remove the catalyst particles and the clear liquor was obtained. The solution was analyzed by a gas chromatograph (GC, Agilent 7890, America). Conversion of aromatic alcohols, yield of aromatic aldehydes, and selectivity for aromatic aldehydes were calculated with following equations:

$$Conversion(\%) = [(C_0\text{-}C_{alcohol})/C_0] \times 100 \qquad (1)$$

$$Yield(\%) = (C_{aldehyde}/C_0) \times 100 \qquad (2)$$

$$Selectivety(\%) = [C_{aldehyde}/(C_0\text{-}C_{alcohol})] \times 100 \qquad (3)$$

Here C_0 is the initial concentration of aromatic alcohols; $C_{alcohol}$ and $C_{aldehyde}$ are the concentrations of the residual aromatic alcohols and the corresponding aromatic aldehydes at a certain time after the catalytic reaction, respectively.

3. Result and discussion

3.1. Catalyst characterization

3.1.1. XRD analysis

The crystallographic structure and phase purity of the as-synthesized samples were investigated by XRD. As shown in Fig. 1, the XRD pattern of $Zn_3In_2S_6$ can be indexed to a hexagonal phase of $Zn_3In_2S_6$ (JCPDS No. 65-4003), which is consistent with the previous report [24]. Furthermore, all diffraction peaks of ZnO are in good agreement with a wurtzite phase of ZnO (JCPDS No. 36-1451). It indicates that the as-prepared $Zn_3In_2S_6$ and ZnO are both of pure phases. Meanwhile, no peaks belonging to ZnO are observed in

$Zn_3In_2S_6$@ZnO sample when the weight ratio of ZnO is 5%. It may be caused by low amount of ZnO in $Zn_3In_2S_6$@ZnO sample. The value of ZnO amount was also measured by ICP-MS. The result showed that the amounts of ZnO in $Zn_3In_2S_6$@5%ZnO, $Zn_3In_2S_6$@10%ZnO and $Zn_3In_2S_6$@15%ZnO samples were 3.6%, 9.2% and 12.8%, respectively. However, in the case of $Zn_3In_2S_6$@10%ZnO and $Zn_3In_2S_6$@15%ZnO samples, the diffraction peaks are well assigned to both of wurtzite phase of ZnO and hexagonal phase of $Zn_3In_2S_6$. Moreover, it is notable that no other new diffraction peaks can be observed in the XRD patterns, indicating that ZnO and $Zn_3In_2S_6$ keep pure phase and no impurities are formed in $Zn_3In_2S_6$@ZnO composites.

3.1.2. SEM and TEM analysis

The morphological structures of the as-prepared $Zn_3In_2S_6$ and $Zn_3In_2S_6$@ZnO composites were investigated by SEM and TEM. As shown in Fig. 2A and B, it is clear that the prepared $Zn_3In_2S_6$ exhibits regular microsphere-like shape with an average diameter of about 1–3 μm. By the further observation, these microspheres with smooth surface were comprised of plentiful petals/sheets. When 5% ZnO was loaded on the $Zn_3In_2S_6$ microspheres, several small nanoparticles can be found to adhere to the surface of $Zn_3In_2S_6$ petals (Fig. S1). It can be seen from Fig. 2C that the morphology of $Zn_3In_2S_6$@10%ZnO sample is also similar to that of $Zn_3In_2S_6$ in general. However, some small nano-fragments (bigger than nanoparticles on $Zn_3In_2S_6$@5%ZnO) can be found to adhere to the surface of petals. And the apparent aggregation of small and big fragments is discerned over $Zn_3In_2S_6$@15%ZnO sample (Fig. 2D). Those fragments are believed to be ZnO. Further investigation was performed by TEM to reveal the hierarchical structure. It can be seen from Fig. 3A that there are not only petals but also some fragments around petals. Moreover, the lattice fringe spacings of petals and fragments are 0.32 nm and 0.25 nm (Fig. 3B), which correspond to (102) and (101) crystal planes of $Zn_3In_2S_6$ and ZnO, respectively. To further clarify the composition profile of the as-synthesized $Zn_3In_2S_6$@ZnO, TEM-mapping analysis was applied. As shown in Fig. 3C, the result indicates that Zn and O enrich the entire microsphere and some fragments loaded on the edge of the microsphere, while In and S distribute in the microsphere. It demonstrates that the assembled ZnO nano-fragments are grown on the whole surface of $Zn_3In_2S_6$ microsphere to form a composite photothermocatalyst.

3.1.3. XPS analysis

XPS was used to further investigate the surface chemical composition and element valence states of $Zn_3In_2S_6$@10%ZnO. As shown in Fig. 4A, the XPS survey spectra shows that there are no other interference peak except Zn, In, S, O and C. The element carbon is probably caused by graphite conductive adhesive. It can be seen from Fig. 4B that the high-resolution spectra of S 2p exist two peaks for S^{2-} at 161.2 eV (S $2p_{3/2}$) and 162.2 eV (S $2p_{1/2}$) [25]. There are double peaks located at 444.8 eV (In $3d_{5/2}$) and 452.4 eV (In $3d_{3/2}$) in Fig. 4C, implying that the valence state of element In is +3 [26]. And two peaks observed at 1021.9 eV and 1045.2 eV (Fig. 4D) belong to Zn^{2+} $2p_{3/2}$ and $2p_{1/2}$, respectively [27]. Moreover, the peaks of O 1s located at 530.7 eV and 530.2 eV (Fig. 4E) are attributed to lattice oxygen in ZnO and the adsorbed oxygen species, respectively [28]. It indicates that the as-synthesized catalyst is composed of pure $Zn_3In_2S_6$ and ZnO. Based on the above characterization, it is concluded that the composite $Zn_3In_2S_6$@ZnO with hierarchical structure could be successfully synthesized by this facile approach.

3.1.4. UV–vis DRS analysis

UV–vis DRS was employed to detect the light absorption properties of the photothermocatalysts. As shown in Fig. 5, it is clear that the absorption edge of $Zn_3In_2S_6$ is about 450 nm, and $Zn_3In_2S_6$@ZnO composites show almost the same visible light absorption as that of $Zn_3In_2S_6$. Compared with absorption
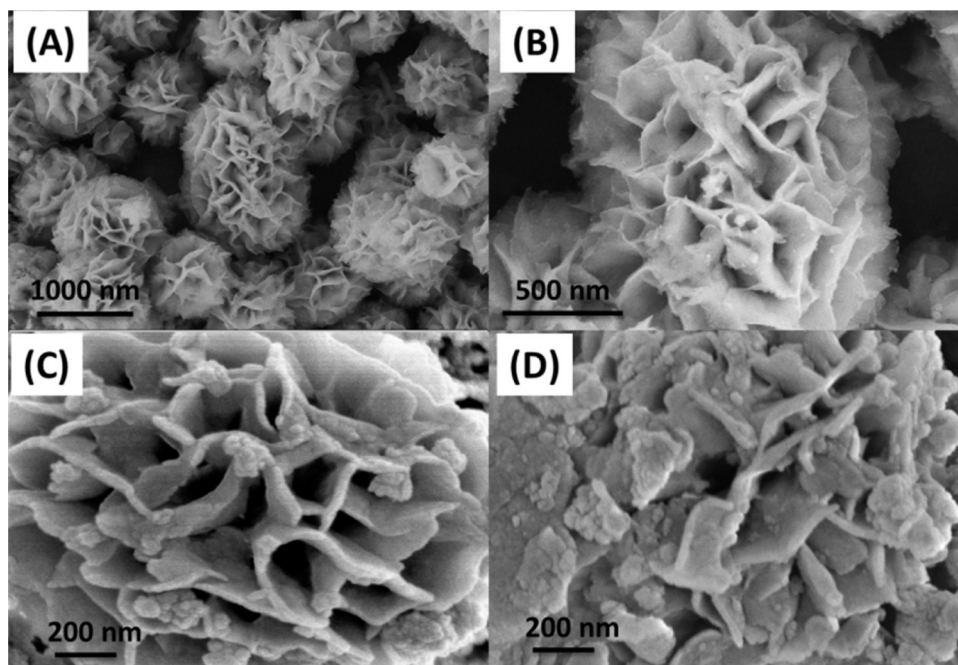
Fig. 2. SEM images of (A and B) $Zn_3In_2S_6$, (C) $Zn_3In_2S_6$@10%ZnO and (D) $Zn_3In_2S_6$@15%ZnO.

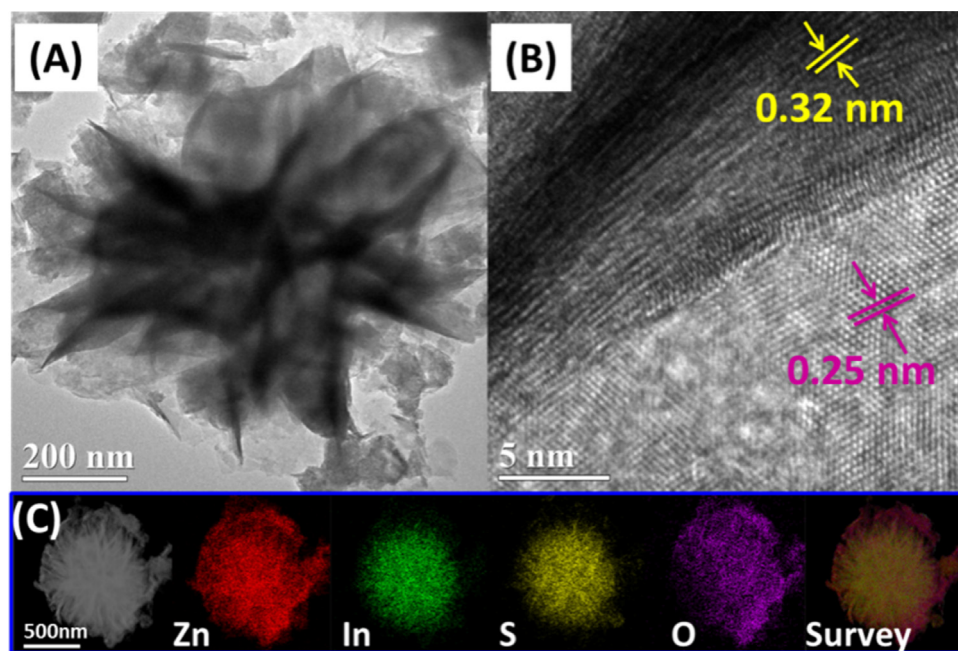**Fig. 3.** (A) TEM, (B) HRTEM and (C) TEM-mapping images of the typical $Zn_3In_2S_6$@15%ZnO composite.

spectrum of $Zn_3In_2S_6$, the stronger absorption of $Zn_3In_2S_6$@ZnO composites in UV region is attributed to the absorption of ZnO. Moreover, the optical band gap energy (E_g) of a direct band semiconductor $Zn_3In_2S_6$ and $Zn_3In_2S_6$@ZnO are calculated from Kubelka-Munk function [29a]: $(\alpha h\nu)^2 = A(h\nu - E_g)$ (α, ν, A and h are the absorption coefficient, light frequency, proportionality and Planck constant, respectively.). As displayed in the inset of Fig. 5, it can be seen that the band gaps of $Zn_3In_2S_6$, $Zn_3In_2S_6$@5%ZnO, $Zn_3In_2S_6$@10%ZnO and $Zn_3In_2S_6$@15%ZnO composites are similar and are about 2.807, 2.817, 2.814 and 2.809 eV, respectively. The difference between the band gaps in these four samples is relatively small, suggesting the optical properties of $Zn_3In_2S_6$ are not

apparently changed by addition of ZnO. It is may be caused by ZnO nano-fragments loaded on surface of $Zn_3In_2S_6$, which possesses high transmission within visible light. In addition, the band edge positions of the valance band (VB) and conduction band (CB) of $Zn_3In_2S_6$ can be determined by the empirical formula [29b]: $E_{CB} = E_{VB} - E_g$; $E_{VB} = X - E_e + 0.5E_g, 0.5E_g$, where E_{CB}, E_{VB}, E_e and X are the conduction band edge, the valance band edge, the energy of free electrons on the hydrogen scale (4.5 eV) and the absolute electronegativity of the semiconductor, respectively. Thus, the E_{VB} and E_{CB} of $Zn_3In_2S_6$ are calculated to be 1.9 and −0.90 eV, respectively. It agrees well with the previous reports [23].
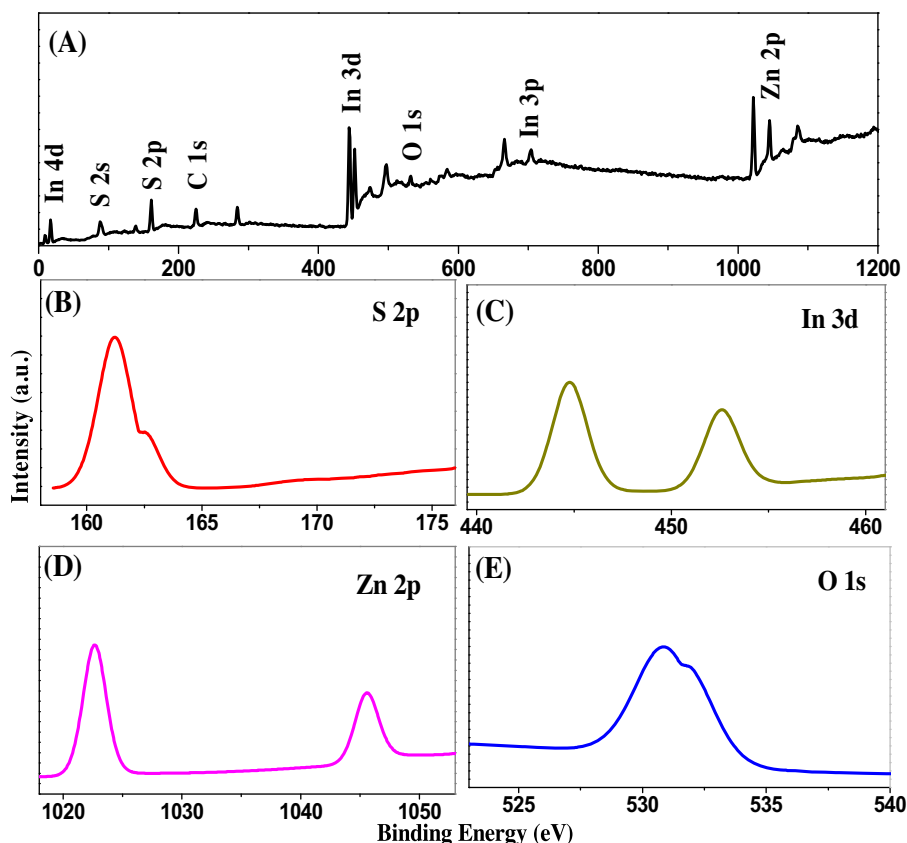
Fig. 4. (A) XPS survey spectra of $Zn_3In_2S_6@10\%ZnO$ and high-resolution spectra of (B) S 2p, (C) In 3d, (D) Zn 2p and (E) O 1 s for the sample.
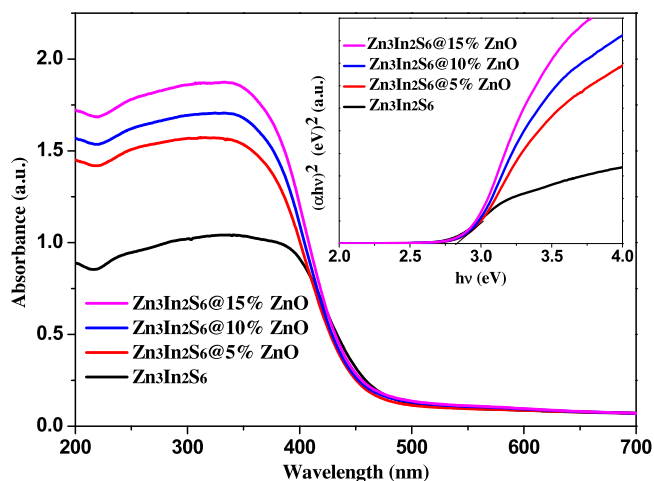

Fig. 5. UV–vis DRS spectra and band gap energies (inset) of the samples.

Fig. 6. N_2 adsorption-desorption isotherms of $Zn_3In_2S_6$ and $Zn_3In_2S_6@10\%ZnO$ composite.

3.1.5. BET analysis

It is known that the surface area is also an important factor for the enhancement of reaction activity. Therefore, the BET (Brunauer-Emmett-Teller) N_2-sorption method was applied to characterize the surface areas of $Zn_3In_2S_6$ and $Zn_3In_2S_6@10\%ZnO$. As shown in Fig. 6, it is clear that both $Zn_3In_2S_6$ and $Zn_3In_2S_6@10\%ZnO$ samples display type IV isotherm with a typical H3 hysteresis loop according to the IUPAC classification [30]. It indicates the presence of unordered mesoporous structure as a result of the hierarchical structure. The specific surface areas of $Zn_3In_2S_6$ and $Zn_3In_2S_6@10\%ZnO$ samples are about 10.4 m²/g and 9.9 m²/g, respectively. The surface areas of the two samples are extremely close. It implies that the effects of specific surface areas on the reaction activity are generally equal.

3.2. Evaluation of catalytic activity

3.2.1. Photocatalytic and photothermocatalytic activities

The activity of the as-prepared $Zn_3In_2S_6$ and $Zn_3In_2S_6@ZnO$ samples were tested by selective oxidation of benzyl alcohol to benzaldehyde under visible light irradiation ($\lambda > 420$ nm). As shown in Fig. 7, it can be seen that the conversion of benzyl alcohol and the yield of benzaldehyde for $Zn_3In_2S_6$ sample are 61.7% and

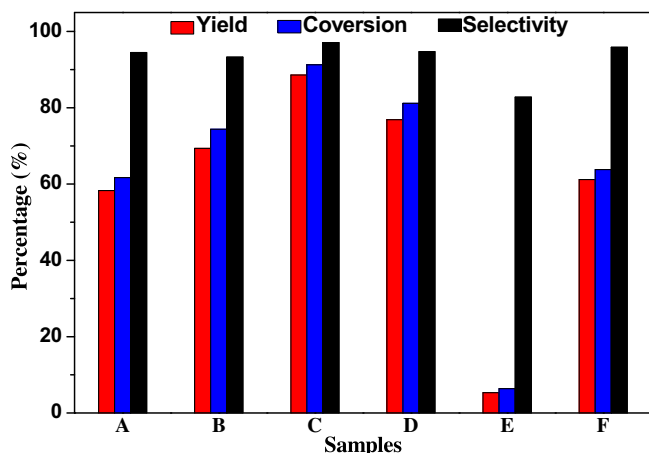**Fig. 7.** The photocatalytic performances of (A) $Zn_3In_2S_6$, (B) $Zn_3In_2S_6$@5%ZnO, (C) $Zn_3In_2S_6$@10%ZnO, (D) $Zn_3In_2S_6$@15%ZnO, (E) ZnO and (F) mechanically mixed $Zn_3In_2S_6$ and 10%ZnO under visible light irradiation for 2 h (the temperature is 323.15 K).

Fig. 8. Yield of selective oxidation of benzyl alcohol to corresponding aldehyde over different catalysts under different temperature with visible light irradiation for 2 h.

58.3% after illumination for 2 h, respectively. Compared with the pure $Zn_3In_2S_6$ sample, both the conversion of benzyl alcohol and the yield of benzaldehyde are increased over all $Zn_3In_2S_6$@ZnO composites. And the optimum amount of ZnO is 10%. When illumination time is 2 h, the conversion of benzyl alcohol and the yield of benzaldehyde are 91.3% and 88.6%, respectively. It has the advantage over other previously reported photocatalysts for photocatalytic selective oxidation of benzyl alcohol into benzaldehyde [12a,13,16–18]. Furthermore, it also can be seen that, for the $Zn_3In_2S_6$ or $Zn_3In_2S_6$@ZnO composites, the selectivity is always steady and higher than 90%. It indicates that $Zn_3In_2S_6$ may be a new alternative photocatalyst for the selective organic transformation under mild conditions. In addition, the catalytic performance of mechanically mixed $Zn_3In_2S_6$-10%ZnO was detected. The result shows that the photocatalytic activity of the mixed sample is apparently lower than that of $Zn_3In_2S_6$@10%ZnO but slightly higher than that of pure $Zn_3In_2S_6$. The result further proved that ZnO and $Zn_3In_2S_6$ integrated more closely in the $Zn_3In_2S_6$@10%ZnO composite than the simple mixture of ZnO and $Zn_3In_2S_6$. Based on the above results, it is clear that ZnO has a significant impact on the catalytic performance of the $Zn_3In_2S_6$@ZnO composites. In order to evaluate the effect of ZnO in the sample, the catalytic performance of ZnO was also evaluated under the same conditions. As shown in Fig. 7, after irradiation for 2 h (the temperature of the reaction system is about 323.15 K), 6.4% benzyl alcohol was converted for pure ZnO sample with 82.8% selectivity. It is known that the wide band gap of ZnO is about 3.2 eV and it can't be motivated by visible light. So, in the experimental condition, ZnO can't exhibit photocatalytic activity. In order to verify the conclusion, the thermocatalytic experiments of ZnO (without light irradiation, the temperature of the reaction system is about 323.15 K) were carried out. The result shows that the conversion of benzyl alcohol is about 6.0% after reaction for 2 h. The result indicates that the conversion of benzyl alcohol is attributed to the thermocatalytic effect of ZnO rather than photocatalytic effect. Meanwhile, the result also shows that no conversion of benzyl alcohol was detected in the blank tests (without catalyst). Based on the results, it is concluded that in the $Zn_3In_2S_6$@ZnO sample, the $Zn_3In_2S_6$ plays a role of the photocatalyst and ZnO plays a role of the thermocatalyst for transforming benzyl alcohol into benzaldehyde. Compared with $Zn_3In_2S_6$ and ZnO samples, the high catalytic activity of $Zn_3In_2S_6$@ZnO should be attributed to the synergistic effect of photocatalysis on $Zn_3In_2S_6$ and low-temperature thermocatalysis on ZnO.

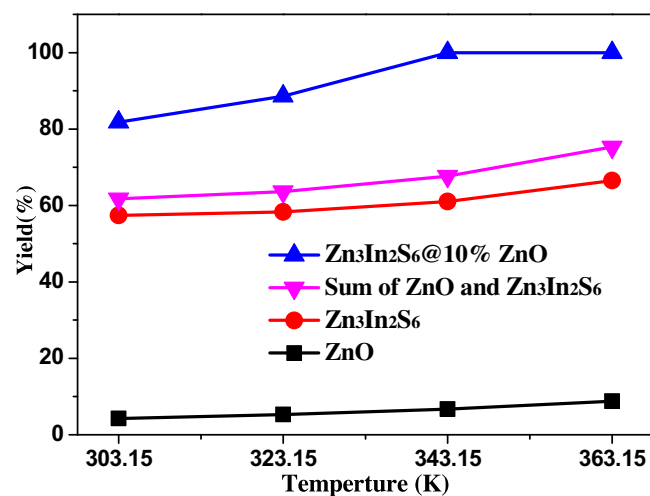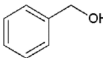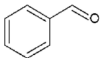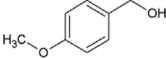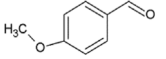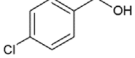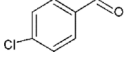In order to further confirm the thermocatalytic activity of ZnO and photothermocatalytic synergistic effect between $Zn_3In_2S_6$ and ZnO for selective transformation of benzyl alcohol into benzaldehyde, the photothermocatalytic test was carried out at different temperatures. As shown in Fig. 8, it c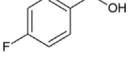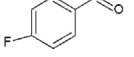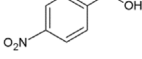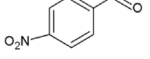an be seen that the yield of benzaldehyde over ZnO is increases gradually with the temperature rising. It indicates that ZnO assuredly can transform benzyl alcohol to benzaldehyde. Furthermore, the increase of reaction temperature is also good for $Zn_3In_2S_6$. It may be caused by the increased collision frequency of molecules in photocatalytic reactions [31]. It should be noted that not any benzaldehyde could be detected over $Zn_3In_2S_6$ at these temperatures (303.15, 323.15, 343.15 and 363.15 K) when visible light irradiation. These indicate that the enhancement of activity of $Zn_3In_2S_6$ is not attributed to thermocatalytic effect. Visible-light-driven photocatalysis is believed to be the primary source of activity of $Zn_3In_2S_6$ for selective transformation of benzyl alcohol into benzaldehyde. Compared with ZnO and $Zn_3In_2S_6$, the $Zn_3In_2S_6$@10%ZnO composite exhibits a dramatic improvement for the transformation of benzyl alcohol into benzaldehyde at each temperature under visible light irradiation. Furthermore, the yield of benzaldehyde over $Zn_3In_2S_6$@10%ZnO is much higher than that of benzaldehyde over $Zn_3In_2S_6$ and benzaldehyde over ZnO. For example, at 343.15 K, the yield of benzaldehyde can reach up to 100% over $Zn_3In_2S_6$@10%ZnO, while the yields of benzaldehyde over ZnO and $Zn_3In_2S_6$ are about 6.7% and 61%, respectively. So the sum value is 67.7%, which is much lower than 100%. Therefore, it can be clearly figured out that the photothermocatalytic activity is not merely the sum of thermocatalytic and photocatalytic activity but some synergistic effect. In a word, the composite $Zn_3In_2S_6$@10%ZnO exhibits notable photothermocatalytic synergistic effect, and the optimal temperature for selective transformation of benzyl alcohol into benzaldehyde is 343.15 K under visible light irradiation. It shows a promising potential application in industrial scale. At the same time, the results also show that, when there is no illumination, the activity of $Zn_3In_2S_6$@ZnO samples is not increased obviously compared with ZnO sample. It also indicates that the $Zn_3In_2S_6$ sample has no thermocatalytic activity again.

3.2.2. Selective oxidation of different aromatic alcohols

In order to extend the general applicability of $Zn_3In_2S_6$@ZnO composite for the selective oxidation of aromatic alcohols to corresponding aromatic aldehydes, a series of aromatic alcohols with different substituent groups were used as substrates. It can be

Table 1
Photocatalytic performances for selective oxidation of aromatic alcohols to corresponding aromatic aldehydes using $Zn_3In_2S_6$ and $Zn_3In_2S_6$@10%ZnO composite at 323.15 K under visible light irradiation for 2 h (Y, C and S mean Yield, Conversion and Selectivity, respectively).

Entry	Substrate	Product	$Zn_3In_2S_6$			$Zn_3In_2S_6$@10% ZnO		
			Y%	C%	S%	Y%	C%	S%
1			58.3	61.7	94.5	88.6	91.3	97
2			83.5	96.1	96.9	100	100	100
3			47.3	49.8	94.7	61.7	65.2	94.6
4			46.2	49.7	93	57.3	62.4	92.1
5			31.4	33.6	93.5	42.8	44.9	95.3

seen from Table 1 that the $Zn_3In_2S_6$@10%ZnO composite exhibits much higher activity than pure $Zn_3In_2S_6$ for selective oxidation of all other aromatic alcohols (p-methoxybenzyl alcohol, p-chlorobenzyl alcohol, p-fluorobenzyl alcohol and p-nitrobenzyl alcohol), it is in accordance with the selective oxidation of benzyl alcohol. In addition, the yields of these aromatic aldehydes are different and present a regular trend (p-methoxybenzyl alcohol > benzyl alcohol > p-chlorobenzylalcohol > p-fluorobenzyl alcohol > p-nitrobenzyl alcohol). It is clear that the yields of aromatic aldehydes decrease with the electron-withdrawing ability of substituent group (the order of electron-withdrawing ability for para-position on benzene is $-OCH_3 < -H < -Cl < -F < -NO_2$). The result is in accordance with the previous reports [18,32], in which the selectivity of photocatalytic oxidation of aromatic alcohols is proportional to the electronegativity of substituent group. The above result indicates that the $Zn_3In_2S_6$@ZnO composite is an excellent catalyst for photothermocatalytic selective transformation of aromatic alcohols to aromatic aldehydes under visible light irradiation.

3.3. Discussion on mechanism

3.3.1. Photoelectrochemical properties

The photoelectronchemical properties (the production capacity and the separation efficiency of photoexcited electron-hole pairs) were detected by an electrochemical workstation. Fig. 9A displays the Photocurrent-Time curves of $Zn_3In_2S_6$ and $Zn_3In_2S_6$@ZnO composites. It is clear that the photocurrent increased rapidly when the light was switched on while the photocurrent declined to base line as the visible light was off. It is known that the photocurrent is produced by diffusion electrons from the separation of the electron-hole pairs motivated by visible light [33]. The pure $Zn_3In_2S_6$ exhibits the highest photocurrent than all the $Zn_3In_2S_6$@ZnO samples. It means more efficient separation and transport of electron-hole pairs of pure $Zn_3In_2S_6$ than that of $Zn_3In_2S_6$@ZnO composites. In other words, compared with $Zn_3In_2S_6$, the loaded ZnO on the $Zn_3In_2S_6$ surface has not contributed to enhancement of separation and transport efficiencies of the photoexcited electron-hole pairs. The electrochemical impedance spectroscopy (EIS) Nyquist plots can further explore the separation efficiency of electron-hole pairs and present the transfer resistance across the solid-liquid junction in the electrode-electrolyte interface region [34]. As shown in Fig. 9B, one arc/semicircle was shown at high frequencies, and a dramatic increase of this frequency arc for $Zn_3In_2S_6$@ZnO composites as compared to $Zn_3In_2S_6$. It indicates
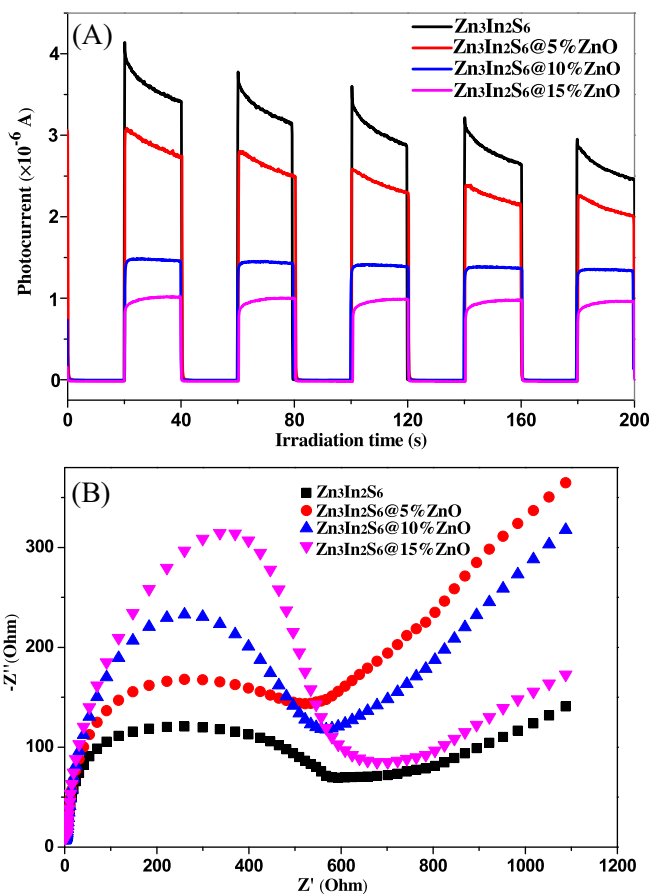
Fig. 9. (A) Transient photocurrent and (B) EIS Nyquist plots of $Zn_3In_2S_6$ and $Zn_3In_2S_6$@ZnO composites in 0.1 M Na_2SO_4 solution and 0.1 M KCl solution containing 0.1 M $K_3[Fe(CN)_6]$/$K_4[Fe(CN)_6]$, respectively.

that $Zn_3In_2S_6$ sample possesses the highest separation efficiency of electron-hole and the fastest interfacial electron transfer. The electrochemical impedance spectroscopy results are in agreement with the conclusion from photocurrent curves.

3.3.2. Photoluminescence analysis

The recombination rate of photoexcited electron-hole pairs was further verified by photoluminescence (PL) emission spectra. Generally, the stronger intensity of PL emission means a higher
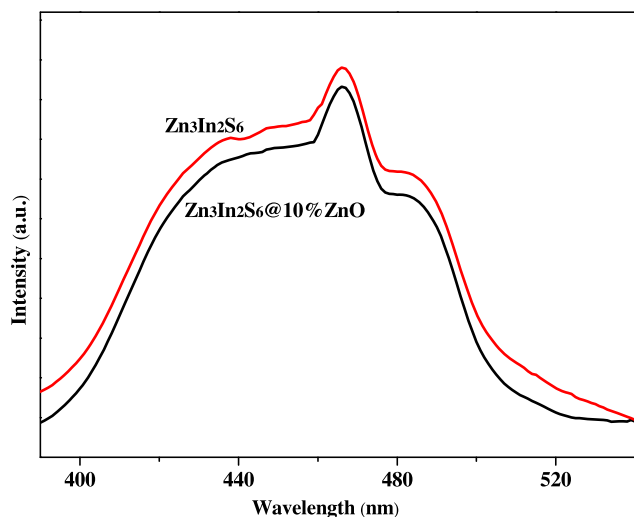
Fig. 10. PL spectra of $Zn_3In_2S_6$ and $Zn_3In_2S_6$@10%ZnO composite.

Fig. 11. Controlled experiments using a series of scavengers on selective oxidation of benzyl alcohol over $Zn_3In_2S_6$@10%ZnO under visible light irradiation for 2 h (the temperature is 323.15 K).

Fig. 12. Proposed reaction mechanism for photothermocatalytic selective oxidation of aromatic alcohols to corresponding aromatic aldehydes.

recombination rate of electrons and holes [18]. As shown in Fig. 10, it is clear that the PL spectra of $Zn_3In_2S_6$ and $Zn_3In_2S_6$@10%ZnO are extremely adjacent; implying that the recombination rate of photoexcited electron-hole pairs of $Zn_3In_2S_6$@10%ZnO composite is nearly the same with that of $Zn_3In_2S_6$. It means that under visible light irradiation, for $Zn_3In_2S_6$@10%ZnO composite, the photogenerated electrons in the conduction band of $Zn_3In_2S_6$ are not migrated to the conduction band of ZnO. In one words, ZnO in the $Zn_3In_2S_6$@10%ZnO composite does not play the function of a photocatalyst.

3.3.3. Role of reactive species

It is known to all that photocatalytic selective oxidation of aromatic alcohols to corresponding aromatic aldehydes are generally generated by superoxide radical ($\bullet O_2^-$), hydroxyl radical ($\cdot OH$) and photogenerated hole (h^+). It is also known that the conduction band position of $Zn_3In_2S_6$ is -0.90 V. The photoexcited electrons of $Zn_3In_2S_6$ can reduce molecular oxygen into $\bullet O_2^-$. In order to clarify the primary reactive species and further deduce the mechanism of selective oxidation of aromatic alcohols to corresponding aromatic aldehydes, a series of control experiments were carried out by adding different radical scavengers. In the study, p-benzoquinone (BQ) [35], triethanolamine (TEOA) [13,36], isopropyl alcohol (IPA) [18,37] and carbon tetrachloride (CCl_4) [13] were introduced as quenchers of $\bullet O_2^-$, h^+, $\cdot OH$ and photogenerated electron (e^-), respectively. The composite $Zn_3In_2S_6$@10%ZnO was taken as a representative of catalysts to detect the roles of different types of reactive species during the process of selective oxidation of benzyl alcohol to corresponding benzaldehyde. As shown in Fig. 11, when BQ was introduced in the reaction system, the conversion of benzyl alcohol reduced apparently and the yield of benzaldehyde also reduced consequently. And a similar phenomenon occurred when CCl_4 was introduced in N_2 reaction system. These indicate that $\bullet O_2^-$ is an important active species in the reaction system. In addition, TEOA is an efficient h^+ scavenger, which leads to the decrease in the yield of benzaldehyde to some extent. However, the yield of benzaldehyde is almost the same with the blank when IPA was added. Therefore, it is concluded that the reaction process is primarily triggered by $\bullet O_2^-$ and h^+, while $\cdot OH$ scarcely interferes with the selective oxidation process.

3.3.4. Proposed photothermocatalytic mechanism

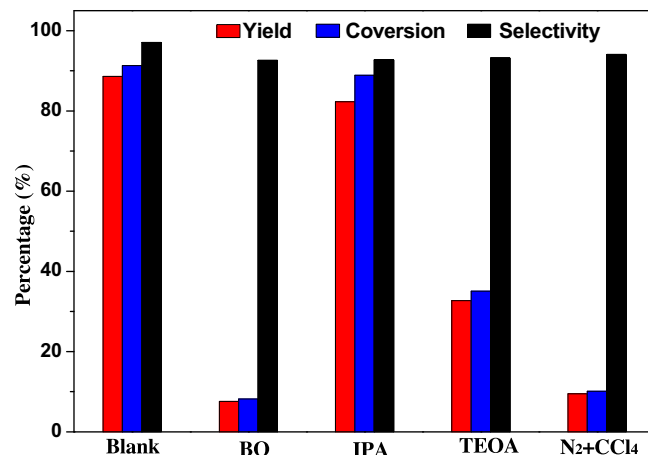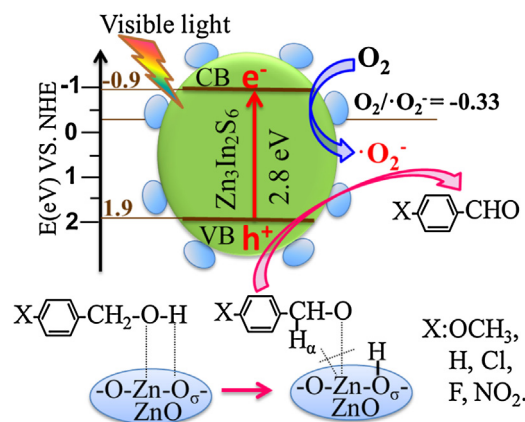On the basis of the above experiment results and analysis, a possible reaction mechanism for photothermocatalytic selective oxidation of aromatic alcohols to corresponding aldehydes over $Zn_3In_2S_6$@ZnO composite was proposed. As shown in Fig. 12, when the $Zn_3In_2S_6$@ZnO composite was irradiated by visible light, the photoexcited electrons and holes are produced in the conduction band (CB) and valence band (VB) of $Zn_3In_2S_6$, respectively. And the photoexcited electrons will be captured by the adsorbed oxygen to generate $\bullet O_2^-$. It is known that $\bullet O_2^-$ and h^+ are the significant reactive species for the photocatalytic selective oxidation of aromatic alcohols to corresponding aldehydes by deprotonation processes. On the other hand, the surface oxygen atom (O_σ) and zinc atom (Zn) of ZnO concertedly interact with the hydrogen (H) and the oxygen of the hydroxy group of alcohol, respectively. The hydrogen of the benzyloxy group (H_α) and H of hydroxy group shift to Zn and O_σ, respectively [38]. As a result, the benzyloxy group ($PhCH_2O-$) and a proton are formed and bound to Zn and O of ZnO, respectively. That is to say, the H_α of the benzyloxy group and H of $-OH$ group interact with ZnO, which weakens bonds of the $C-H_\alpha$ and the $O-H$. Then, it is easy for the reactive species ($\bullet O_2^-$ and h^+) to react with the H_α and the H of $-OH$ group to produce benzaldehyde and H_2O. Therefore, compared with the photocatalytic reaction of $Zn_3In_2S_6$ and the thermocatalytic reaction of ZnO, the $Zn_3In_2S_6$@ZnO composite exhibits remarkable activity for the selective oxidation of aromatic alcohols to corresponding aromatic aldehydes under mild reaction conditions.
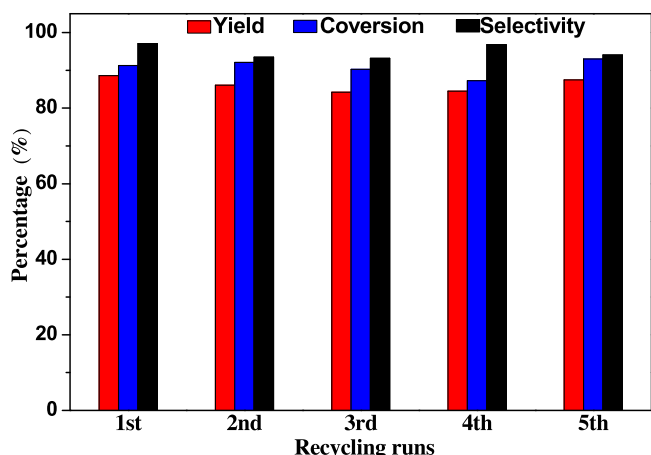
Fig. 13. Cyclic experiments of Zn3In2S6@10%ZnO sample for the selective oxidation of benzyl alcohol under visible light irradiation (the temperature is 323.15 K).
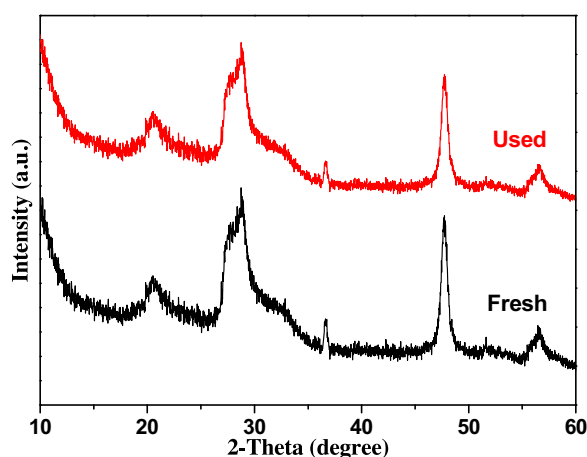

Fig. 14. XRD patterns of fresh and used Zn3In2S6@10%ZnO after photocatalytic reaction.

3.4. Stability of catalyst

The stability of catalyst is important for its extensive application in industry. In the study, the $Zn_3In_2S_6$@10%ZnO composite with the highest reaction activity is selected as a sample to detect the catalyst's reusability in repeated experiments under the same conditions. The $Zn_3In_2S_6$@10%ZnO sample was centrifuged after each cycle of the reactions and purged totally with deionized water and ethanol. After being dried, the obtained sample was reacted with fresh reactants, and the progress will be continued for five cycles. As shown in Fig. 13, it can be seen that after five successive cycles, the conversion rate of benzyl alcohol, yield of benzaldehyde and selectivity of oxidation process are the same. It indicates that the reaction activity of $Zn_3In_2S_6$@10%ZnO composite has not been weakened in the experimental conditions. Moreover, the XRD patterns of $Zn_3In_2S_6$@10%ZnO sample used for 5 times and the fresh sample are almost identical (Fig. 14). These indicate that $Zn_3In_2S_6$@10%ZnO composite is a stable catalyst driven by visible light for selective oxidation of benzyl alcohol to corresponding aldehyde.

4. Conclusions

In summary, a new type photothermocatalyst $Zn_3In_2S_6$@ZnO which combines photocatalyst of $Zn_3In_2S_6$ and low-temperature thermocatalyst of ZnO has been successfully prepared. Compared with the photocatalytic activity of $Zn_3In_2S_6$ and thermocatalytic activity of ZnO, the $Zn_3In_2S_6$@ZnO composite exhibits a dramatic enhanced activity for the selective oxidation of benzyl alcohol into benzaldehyde under visible light irradiation. The increased activity of the $Zn_3In_2S_6$@ZnO composite should be attributed to the synergetic effect between the photocatalysis on $Zn_3In_2S_6$ and thermocatalysis on ZnO. The $Zn_3In_2S_6$@ZnO composite exhibits remarkable stability and promising potential application in industrial scale. In the reaction, the bonds of the C—H$_\alpha$ and the O—H can be weakened via thermocatalytic interaction of the thermocatalyst ZnO, and the reactive species ($\bullet O_2^-$ and h$^+$) can be generated by the photocatalytic reaction of $Zn_3In_2S_6$. The synergistic effect of photocatalysis on $Zn_3In_2S_6$ and low-temperature thermocatalysis on ZnO leads to enhanced activity. This study provides a promising way to design novel and efficient visible-light-driven photothermocatalyst for selective oxidation of aromatic alcohols or other organics under mild reaction conditions.

Acknowledgements

Appendix A. Supplementary data

Supplementary data associated with this article can be found, in the online version, at http://dx.doi.org/10.1016/j.apcatb.2017.06.078.

References

[1] A. Fujishima, K. Honda, Nature 238 (1972) 37–38.
[2] (a) M.R. Hoffmann, S.T. Martin, W. Choi, D.W. Bahnemann, Chem. Rev. 95 (1995) 69–96;
(b) A.H. Mamaghani, F. Haghighat, C.-S. Lee, Appl. Catal. B Environ. 203 (2017) 247–269;
(c) M. Zhang, C. Chen, W. Ma, J. Zhao, Angew. Chem. 120 (2008) 9876–9879.
[3] (a) A. Kudo, Y. Miseki, Chem. Soc. Rev. 38 (2009) 253–278;
(b) N. Zhang, Y. Zhang, M. Yang, Z. Tang, Y. Xu, J. Catal. 299 (2013) 210–221.
[4] X.C. Wang, K. Maeda, A. Thomas, K. Takanabe, G. Xin, J.M. Carlsson, K. Domen, M. Antonietti, Nat. Mater. 8 (2009) 76–80.
[5] P. Zhou, J. Yu, M. Jaroniec, Adv. Mater. 26 (2014) 4920–4935.
[6] H. Wang, L. Zhang, Z. Chen, J. Hu, S. Li, Z. Wang, J. Liu, X. Wang, Chem. Soc. Rev. 43 (2014) 5234–5244.
[7] (a) N. Zhang, M.-Q. Yang, S. Liu, Y. Sun, Y.-J. Xu, Chem. Rev. 115 (2015) 10307–10377;
(b) K. Wenderich, G. Mul, Chem. Rev. 116 (2016) 14587–14619.
[8] (a) Y. Wang, H. Dai, J. Deng, Y. Liu, H. Arandiyan, X. Li, B. Gao, S. Xie, Solid State Sci. 24 (2013) 62–70;
(b) Y. Wang, H. Dai, J. Deng, Y. Liu, Z. Zhao, X. Li, H. Arandiyan, Chem. Eng. J. 226 (2013) 87–94;
(c) Z. Zhao, H. Dai, J. Deng, Y. Liu, Y. Wang, X. Li, G. Bai, B. Gao, C.T. Au, J. Environ. Sci. 25 (2013) 2138–2149.
[9] (a) X. Lang, X.J. Chen Zhao, Chem. Soc. Rev. 43 (2014) 473–486;
(b) X. Lang, J. Zhao, X. Chen, Chem. Soc. Rev. 45 (2016) 3026–3038;
(c) J.C. Colmenares, R. Luque, Chem. Soc. Rev. 43 (2014) 765–778;
(d) C. Zheng, G. He, X. Xiao, M. Lu, H. Zhong, X. Zuo, J. Nan, Appl. Catal. B Environ. 205 (2017) 201–210.
[10] (a) C. Stephenson, T. Yoon, Acc. Chem. Res. 49 (2016) 2059–2060;
(b) M. Majek, A.J. Wangelin, Acc. Chem. Res. 49 (2016) 2316–2327.
[11] T. Mallat, A. Baiker, Chem. Rev. 104 (2004) 3037–3058.
[12] (a) M. Zhang, Q. Wang, C. Chen, L. Zang, W. Ma, J. Zhao, Angew Chem. 121 (2009) 6197–6200;
(b) S. Patel, B.K. Mishra, J. Org. Chem. 71 (2006) 6759–6766;
(c) J.A. Mueller, M.S. Sigman, J. Am. Chem. Soc. 126 (2004) 9724–9734.
[13] X. Xiao, J. Jiang, L. Zhang, Appl. Catal. B Environ. 142-143 (2013) 487–493.
[14] D.I. Enache, J.K. Edwards, P. Landon, B. Solsona-Espriu, A.F. Carley, A.A. Herzing, M. Watanabe, C.J. Kiely, D.W. Knight, G.J. Hutchings, Science 311 (2006) 362–365.
[15] (a) J. Fan, Y. Dai, Y. Li, N. Zheng, J. Guo, X. Yan, G.D. Stucky, J. Am. Chem. Soc. 131 (2009) 15568–15569;
(b) J. Wang, P. Rao, W. An, J. Xu, Y. Men, Appl. Catal. B Environ. 195 (2016) 141–148.
[16] Y. Zhang, Z. Tang, X. Fu, Y. Xu, ACS Nano 5 (2011) 7426–7435.

[17] Z. Chen, J. Xu, Z. Ren, Y. He, G. Xiao, Catal. Commun. 41 (2013) 83–86.
[18] S. Meng, X. Ye, X. Ning, M. Xie, X. Fu, S. Chen, Appl. Catal. B Environ. 182 (2016) 356–368.
[19] B. Long, Z. Ding, X. Wang, ChemSusChem 6 (2013) 2074–2078.
[20] W.H. Cheng, S. Akter, H.H. Kung, J. Catal. 82 (1983) 341–350.
[21] M.V. Morales, E. Asedegbega-Nieto, A. Iglesias-Juez, I. Rodríguez-Ramos, A. Guerrero-Ruiz, ChemSusChem 8 (2015) 2223–2230.
[22] Y. Shinohara, T. Nakajima, S. Suzuki, J. Mol. Struct. 460 (1999) 231–244.
[23] (a) J. Song, C. Ma, W. Zhang, S. Yang, S. Wang, L. Lv, L. Zhu, R. Xia, X. Xu, J. Mater. Chem. B 4 (2016) 7909–7918;
(b) I. Poulios, N. Papadopoulos, Sol. Energy Mater. 20 (1990) 43–51.
[24] S. Shen, L. Zhao, L. Guo, Int. J. Hydrog. Energy 35 (2010) 10148–10154.
[25] Z. Chen, Y.J. Xu, ACS Appl. Mater. Interfaces 5 (2013) 13353–13363.
[26] (a) C.W. Tan, G.Q. Zhu, M. Hojamberdiev, K.S. Lokesh, X.C. Luo, L. Jin, J.P. Zhou, P. Liu, J. Hazard. Mater. 278 (2014) 572–583;
(b) L. Yuan, M.Q. Yang, Y.J. Xu, J. Mater. Chem. A 2 (2014) 14401–14412.
[27] Q. Liu, H. Lu, Z.W. Shi, F.L. Wu, J. Guo, K.M. Deng, L. Li, ACS Appl. Mater. Interfaces 6 (2014) 17200–17207.
[28] (a) G. Zhou, D.W. Wang, L. Li, N. Li, F. Li, H.M. Cheng, Nanoscale 5 (2013) 1576–1582;
(b) S. Cavaliere, S. Subianto, I. Savych, M. Tillard, D.J. Jones, J. Roziere, J. Phys. Chem. C 117 (2013) 18298–18307.
[29] (a) S. Sakthivel, H. Kisch, Angew. Chem. Int. Ed. 42 (2003) 4908–4911;
(b) M.A. Butler, D.S. Ginley, J. Electrochem. Soc. 125 (1978) 228–232.
[30] K.S. Sing, Pure Appl. Chem. 57 (1985) 603–619.
[31] (a) M.-C. Lu, G.D. Roam, J.-N. Chen, C.P. Huang, J. Photochem. Photobiol. A: Chem. 76 (1993) 103–110;
(b) E. Evgenidou, K. Fytianos, I. Poulios, Appl. Catal. B Environ. 59 (2005) 81–89.
[32] (a) T. Punniyamurthy, S. Velusamy, J. Iqbal, Chem. Rev. 105 (2005) 2329–2363;
(b) N. Zhang, M.-Q. Yang, Z.-R. Tang, Y.-J. Xu, J. Catal. 303 (2013) 60–69.
[33] (a) S. Soedergren, A. Hagfeldt, J. Olsson, S.E. Lindquist, J. Phys. Chem. 98 (1994) 5552–5556;
(b) H.W. Han, X.Z. Zhao, J. Liu, J. Electrochem. Soc. 152 (2005) A164–A166.
[34] (a) N. Li, G. Liu, C. Zhen, F. Li, L.L. Zhang, H.M. Cheng, Adv. Funct. Mater. 21 (2011) 1717–1722;
(b) Z. Hosseini, N. Taghavinia, N. Sharifi, M. Chavoshi, M. Rahman, J. Phys. Chem. C 112 (2008) 18686–18689.
[35] R. Palominos, J. Freer, M.A. Mondaca, H.D. Mansilla, J. Photochem. Photobiol. A 193 (2008) 139–145.
[36] S.C. Yan, Z.S. Li, Z.G. Zou, Langmuir 26 (2010) 3894–3901.
[37] M. Sadakane, K. Sasaki, H. Kunioku, B. Ohtani, W. Ueda, R. Abe, Chem. Commun. 48 (2008) 6552–6554.
[38] Y. Iwasawa, Acc. Chem. Res. 30 (1997) 103–109.